Electronic Supplementary Information for

Elimination of Grain Boundary Resistance in Vanadoborate Electrolyte via the Hydrogen-Bond Interaction of Glycerol

Shan Zhang,[ab] Ying Lu,*[a], Xiu-Wei Sun,[a] Hong-Rui Tian,[a] Xue Bai,[a] Shu-Xia Liu*[a]

[a.] Key Laboratory of Polyoxometalate and Reticular Material Chemistry of Ministry of Education, College of Chemistry, Northeast Normal University, Changchun 130024, China. E-mail: liusx@nenu.edu.cn, luy968@nenu.edu.cn.

[b.] School of Chemical and Environmental Engineering, Liaoning University of Technology, Jinzhou 121001, PR China.

Contents

1. Experimental Section

1.1 Materials and Instrumentations

All solvents and reagents are obtained from commercial sources and used without further purification.

Fourier transform infrared (FT-IR) spectra were analyzed between 500-4000 cm^{-1} on an Alpha Centaurt spectrophotometer. The crystallographic orientation of **VB** is indexed by X-ray diffractometer (Bruker Smart Apex CCD) with Mo-Kα radiation. Water vapor adsorption/desorption isotherms were performed on Hiden isochema IGA 100B instrument at 298 K. Impedance Analyses were carried out on Solartron SI 1260 impedance/gain phase analyzer with an AC voltage of 50 mV and an AC frequency $0.1-10^6$ Hz. The relative humidity and temperature environment required by the sample during proton conduction test are adjusted through Memmert HCP108 constant temperature and humidity chamber. Cyclic voltammetry (CV) study was conducted on a CHI660E electrochemical workstation in a three-electrode system: saturated calomel electrode as reference electrode, platinum as the counter electrode, and **VB-Gl-1.3%** modified carbon paste electrodes was used as the working electrode.

1.2 Synthesis of $\{[Cd(H_2O)_2]_3V_{12}B_{18}O_{54}(OH)_6\}\cdot 4H_3O\cdot 26H_2O$ (VB)

Based on the previously reported method, a slightly modified hydrothermal method was used to synthesize **VB**. Briefly, $[Cd(CH_3COO)_2\cdot 2H_2O]$ (0.028 g, 0. 11 mmol), $V(acac)_3$ (0.122 g, 0.35 mmol) and H_3BO_3 (0.308 g, 5.00 mmol) were dissolved in the mixture of 0.1 mL monoethanolamine and 2.5 mL deionized water. The mixture was stirred for 0.5 h, then sealed in the Teflon reactor and heated at 100 °C for 7 days. After cooling slowly to room temperature, a millimeter grade violet black crystal **VB** with rhomboid dodecahedron was obtained. The crystals were fully washed with deionized water and then dried at room temperature with a yield of 74%, based on $V(acac)_3$. The phase purity was confirmed by power XRD analysis.

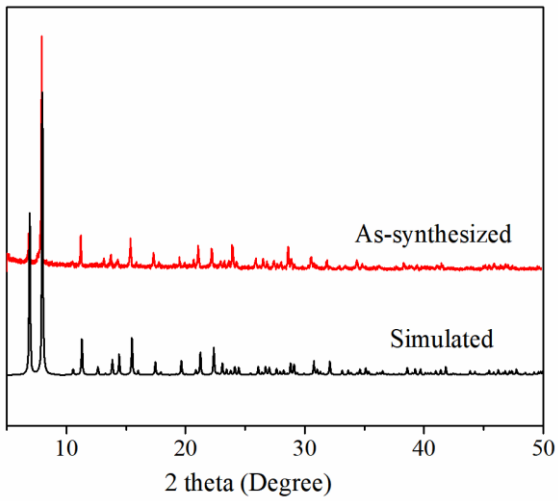

Power XRD profiles of **VB** sample.

1.3 Preparation of composites VB-Gl-x

A series of composites based on different Gl addition were prepared by physical blending. The specific operation process is as follows: 1.00 g **VB** is mixed with different masses of Gl (0.003 g, 0.005 g, 0.010 g and 0.013 g) respectively, and the evenly composites are obtained by mechanical grinding, which are named **VB-Gl-x** (x represents the mass percentage of Gl in **VB**).

Given that vanadoborate has a 3D porous structure, initially we wondered whether glycerol exists only in the interparticle space or in both the interparticle space and the holes of vanadoborate single crystal. Therefore, we conducted additional experiments to investigate this question. Immersed vanadoborate single crystal in a 1:1 volume ratio of glycerol and H_2O solution for one week, then separated the single crystal samples (named **Gl@VB)**. Then, the FT-IR spectra and single crystal X-ray diffraction data analysis of **Gl@VB** were carried out. The results showed that no -CH_2- symmetric stretching vibration peaks belonging to glycerol molecules were observed at about 2870 and 2930 cm^{-1}, and the IR spectrum of **Gl@VB** is almost completely coincident with that of **VB**. In addition, the single crystal data proves once again that there are no glycerol molecules in the pores of **VB**. Therefore, we think that glycerol molecules are difficult to enter the pores of vanadate single crystals, and only exist in the gaps of single crystals for the prepared composite.

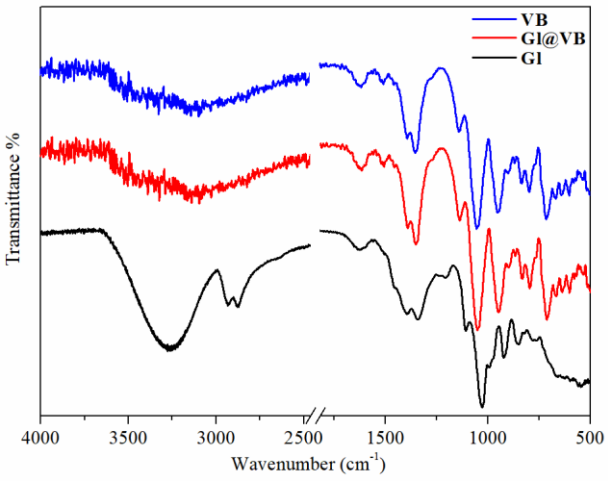

IF-IR spectra of **VB**, Gl and **Gl@VB**.

1.4 Proton Conductivity Measurements.

The proton conduction of all samples in this paper was carried out using the double probe method. The resistance value R was obtained by equivalent circuit fitting using Zview software. The conductivity value is calculated by the equation:

$$\sigma = \frac{L}{R \times S}$$

Where L and S are the effective measurement length (cm) and cross-sectional area (cm^2) of the test sample, respectively. σ is the proton conductivity (S cm^{-1}).

Proton Conduction of VB Pellet Sample.

The synthesized **VB** samples were ground into powder in a mortar and pressed into a tablet with a thickness of about 0.05–0.07 cm (measured with a vernier caliper) in a mold with a diameter of 0.8 cm. The sample tablet is clamped between two copper-plated electrode clamps with conductive leads, then placed in a constant temperature and humidity chamber, and the AC impedance test at the selected relative humidity and temperature is performed.

Proton Conduction Measurement of VB Single Crystal.

The anisotropic proton conductivity of single crystal **VB** was studied using the traditional double-contact wire bonding method. Firstly, the [100] and [110] directions of single crystal samples were indexed by Bruker Smart Apex CCD diffraction, and then conductive silver glue was used to carefully coating the two parallel planes tangent to the [100] or [110] directions, namely {100} and {110} crystal planes, respectively. Furthermore, it was connected to the self-made electrode through a soft silver wire (0.1 mm), dried at room temperature for 24 h and tested for AC impedance. To ensure the accuracy of single crystal proton conductivities, at least 5 crystal samples are tested in each direction. The effective length and cross-sectional area of the tested crystal were calculated by X-ray diffraction and **VB**'s unique rhombic dodecahedron structure.

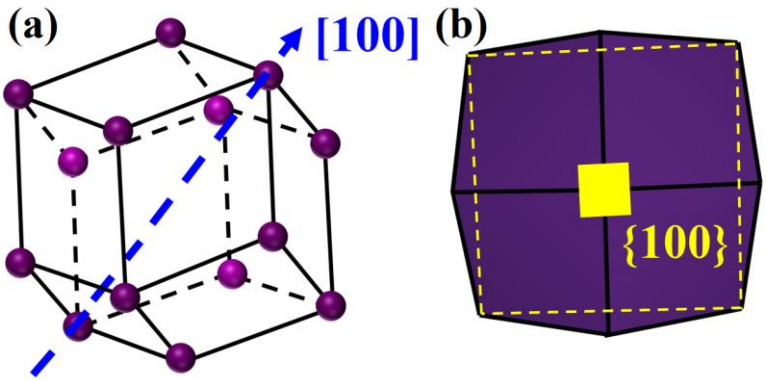

(a) Crystal model of **VB** rhombic dodecahedron; (b) The {100} crystallographic planes (yellow solid line) is given for crystal morphology. The dashed line represents the effective region of conductive adhesive bonding in the [100] direction conductivity test.

2. Analysis of VB structure-conductivity relationship

In **VB**, typical closed-shell $[V_{12}B_{16}O_{54}(OH)_6(H_2O)]^{10-}$ clusters are connected by $[Cd(H_2O)_2]^{2+}$ cationic units to form a 3D framework with cross channels in the *a*, *b* and *c* axis directions. Along [100] direction, there are two types of channels (type A and B) situated by H_3O^+ and H_2O. In type A channel, a water molecule chain is formed by crystal water molecules O4W and O5W and coordination water molecules O2W and O3W from Cd(II) by hydrogen bonds with O···O distances from 2.518 to 3.038 Å. Moreover, there are complicated hydrogen bonds interactions among the hydrophilic O^{2-}/OH^- groups in the wall of the channel and the water molecule chain, resulting dense and continuous hydrogen bond network. In type B channel, crystal water molecules O5W and coordination water molecules O3W of Cd(II) form a $(H_2O)_8$ cluster, yet there is no H-bond interaction between adjacent $(H_2O)_8$ clusters. So, the H-bond network within type A channel is the preferred proton conduction pathway along [100] direction. However, there is no channel along [110] direction, and the hydrogen bond network is formed by coordination water molecules O2W, O3W and hydrophilic O^{2-}/OH^- groups of $[V_{12}B_{16}O_{54}(OH)_6(H_2O)]^{10-}$ clusters (O···O = 2.428~3.199 Å). Base on the above analysis, we can conclude that the possible proton conduction pathways along [100] and [110] directions have two significant distinctions: one is the proton donors include H_3O^+ and coordination water molecule along [100] direction, while coordination water molecule is the sole proton donor along [110] plane; the other is that crystal water molecules are mainly components of proton conduction pathway along [100] direction, while crystal water molecules are absent in the proton conduction pathway along (110)

plane. The weaker acidity of proton donated by coordination water molecule may explicate the obviously lower conductivity along [110] direction than that of [100] direction. Moreover, the differences in the conductivity's humidity dependences as well conductivity's changes with the increased temperature after 55 °C along [110] and [100] directions are also well explained by the presence or not of crystal water molecules in their proton conduction pathway. Crystal water molecule is more likely to loss than coordination water molecule under low humidity or high temperature conditions.

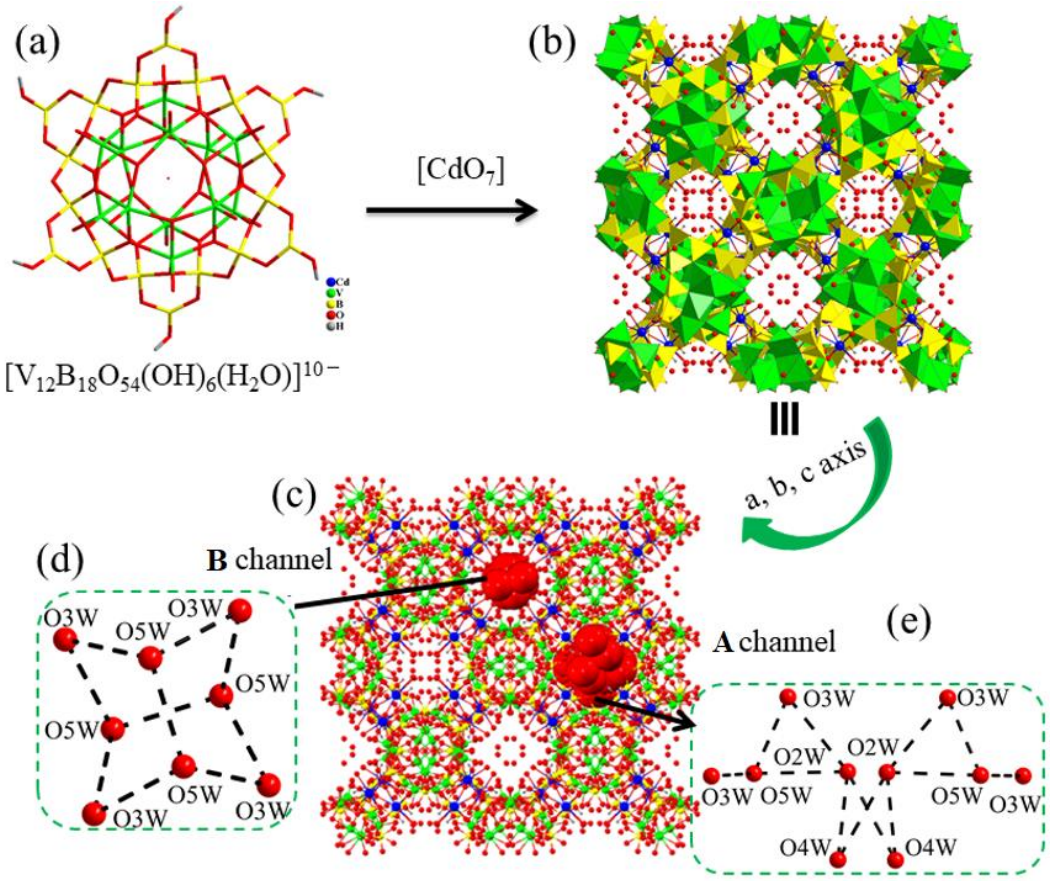

(a) The structure of the $[V_{12}B_{16}O_{54}(OH)_6(H_2O)]^{10-}$ cluster; (b) A 3D open framework connected by $[CdO_7]$ and $[V_{12}B_{16}O_{54}(OH)_6(H_2O)]^{10-}$; (c–e) A, B channels within the framework and different aggregates of water molecules.

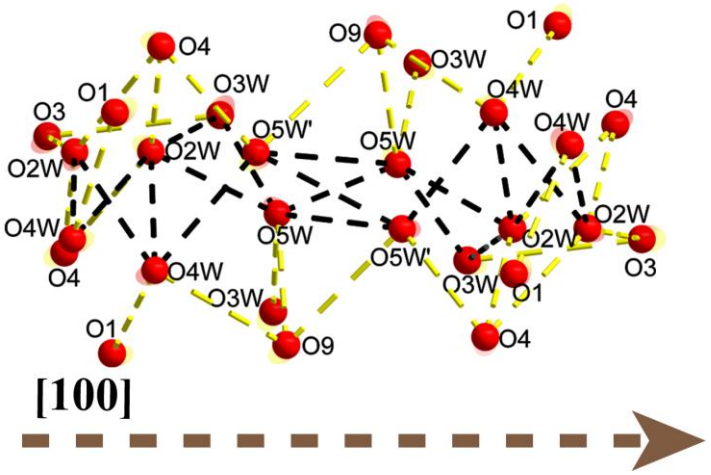

Schematic representation of the possible proton transfer along the [100] direction by hydrogen bond interaction.

Table The distance between the non-hydrogen atoms in the hydrogen bond formed between the coordination water and the crystal water molecule within the A channel of [100] direction.

Atoms involved	Length (Å)	Atoms involved	Length (Å)
O5W···O5W′	3.038	O4W···O2W	3.016
O5W′···O5W′	3.008	O4W···O5W′	2.939
O2W···O3W	2.883	O2W···O5W	2.785
O2W···O4W	2.649	O3W···O5W	2.518

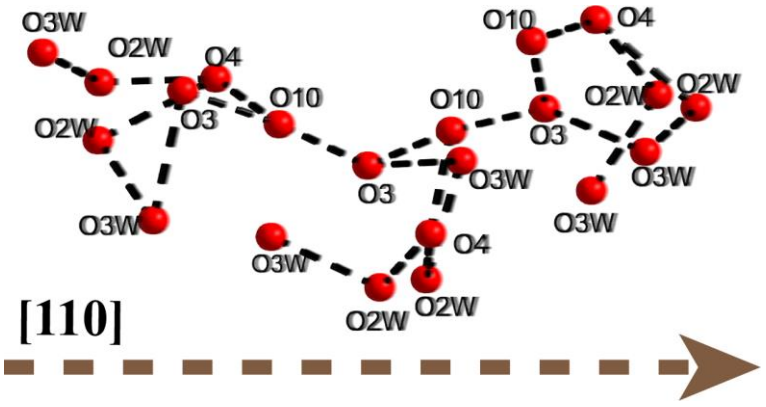

Schematic representation of the possible proton transfer along the [110] direction by hydrogen bond interaction.

Table The distance between the non-hydrogen atoms in the hydrogen bond formed between the coordination water and hydrophilic O^{2-}/OH^{-} groups of $[V_{12}B_{16}O_{54}(OH)_6(H_2O)]^{10-}$ clusters in the [110] direction.

Atoms involved	Length (Å)	Atoms involved	Length (Å)
O3W···O3	3.199	O2W···O4	3.104
O3W···O2W	2.883	O2W···O4	2.676
O3···O10	2.439	O4···O10	2.437
O3···O10	2.428		

3. Supplementary Figures

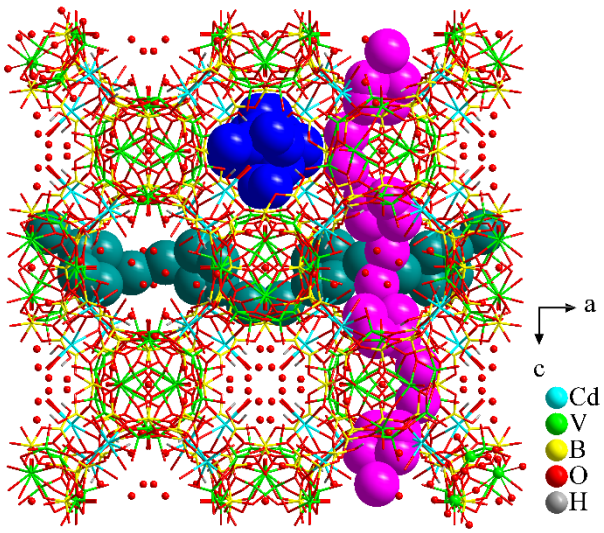

Fig. S1 The three-dimensional structure with interconnected channels filled with a large amount of H_3O^+ and H_2O (the pink, blue and teal balls also represent water molecules).

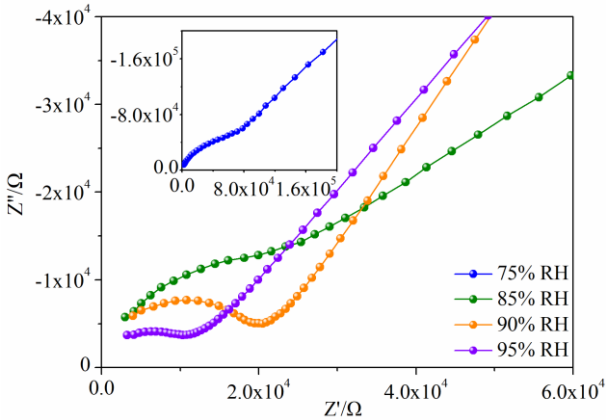

Fig. S2 Nyquist plots of **VB** powder sample under different relative humidity at 25 ℃.

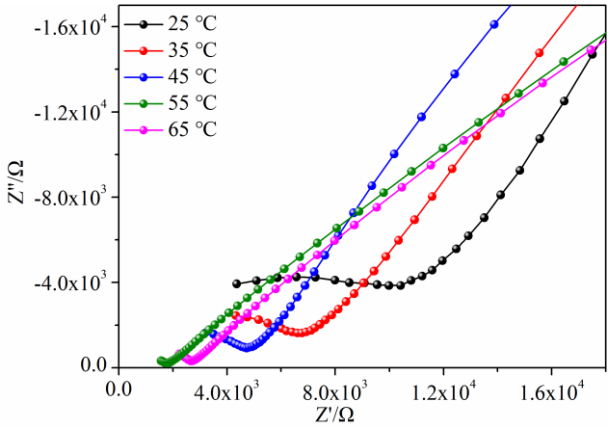

Fig. S3 Nyquist plots of **VB** powder sample under 95% RH and different temperatures.

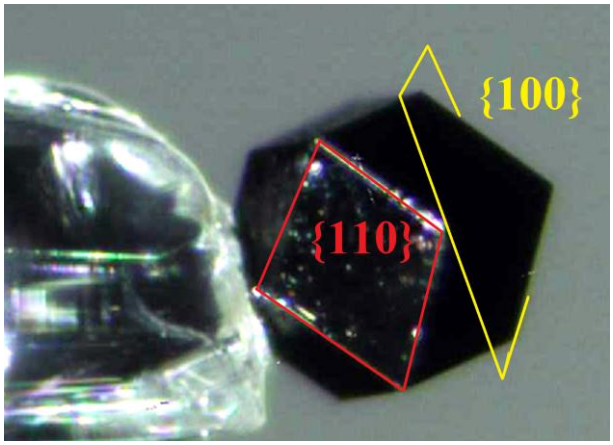

Fig. S4 The rhombohedral shape of **VB**, and {100} and {110} crystal surfaces as directed by single-crystal X-ray diffraction technique.

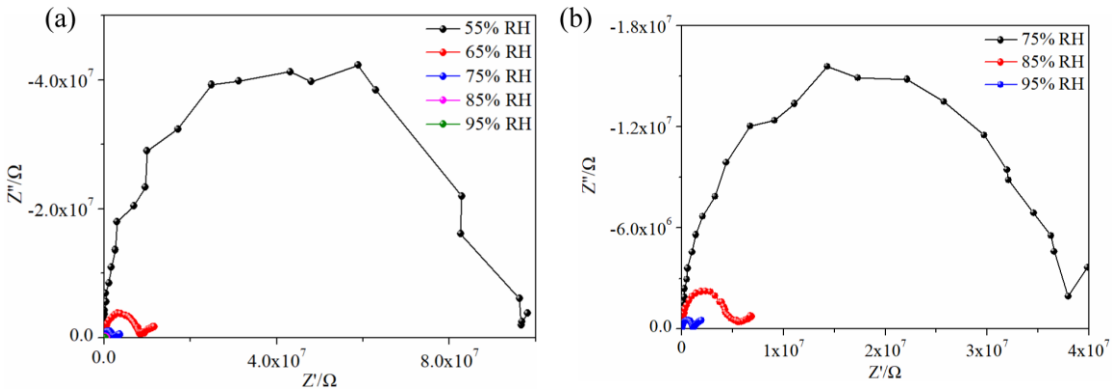

Fig. S5 Nyquist plots of single crystal **VB** along (a) [100] and (b) [110] directions at 25 ℃ and different relative humidity.

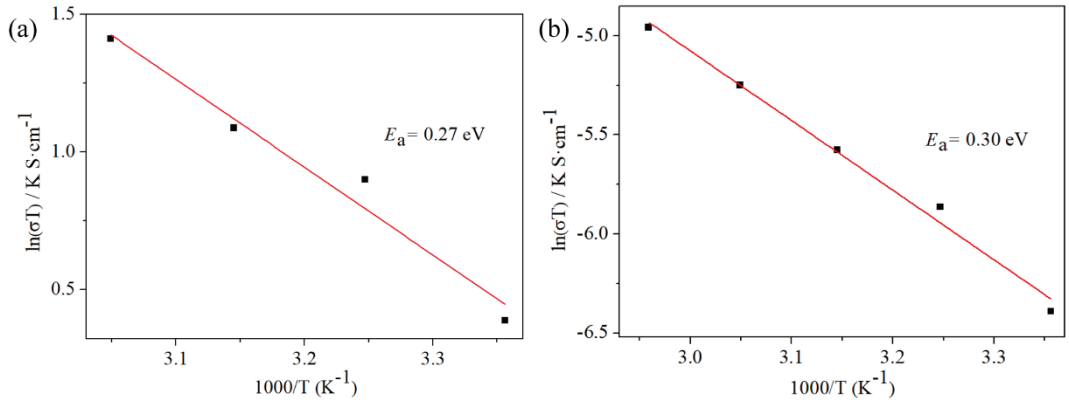

Fig. S6 Arrhenius plot of the proton conductivity for (a) [100] and (b) [110] directions.

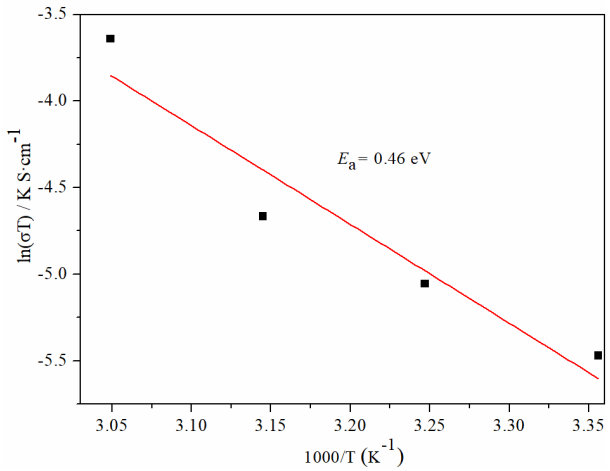

Fig. S7 Arrhenius plot of the proton conductivity for **VB**.

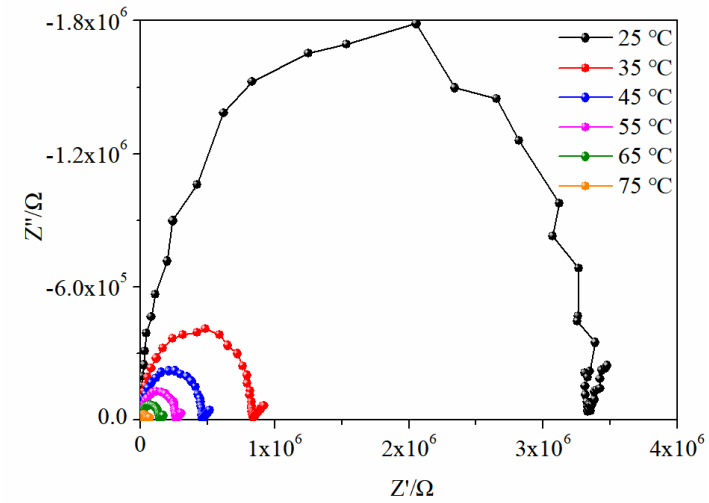

Fig. S8 Nyquist curves of Gl at 95% RH and various temperatures.

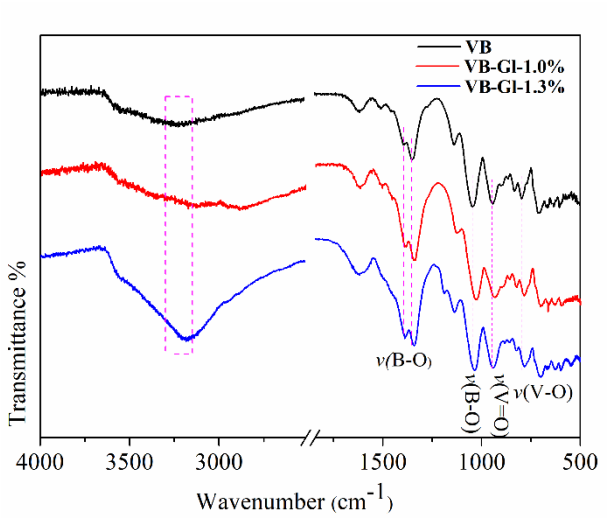

Fig. S9 FT-IR spectra of **VB**、**VB-Gl-1.0%** and **VB-Gl-1.3%**.

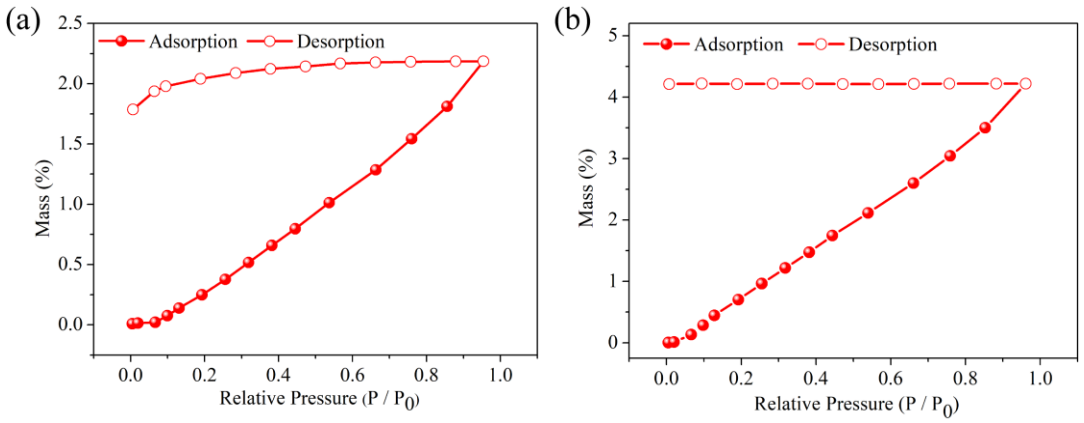

Fig. S10 Water adsorption (filled circles) and desorption (open circles) isotherms of **VB** and **VB-Gl-1.3%** in tablet state at 25 ℃.

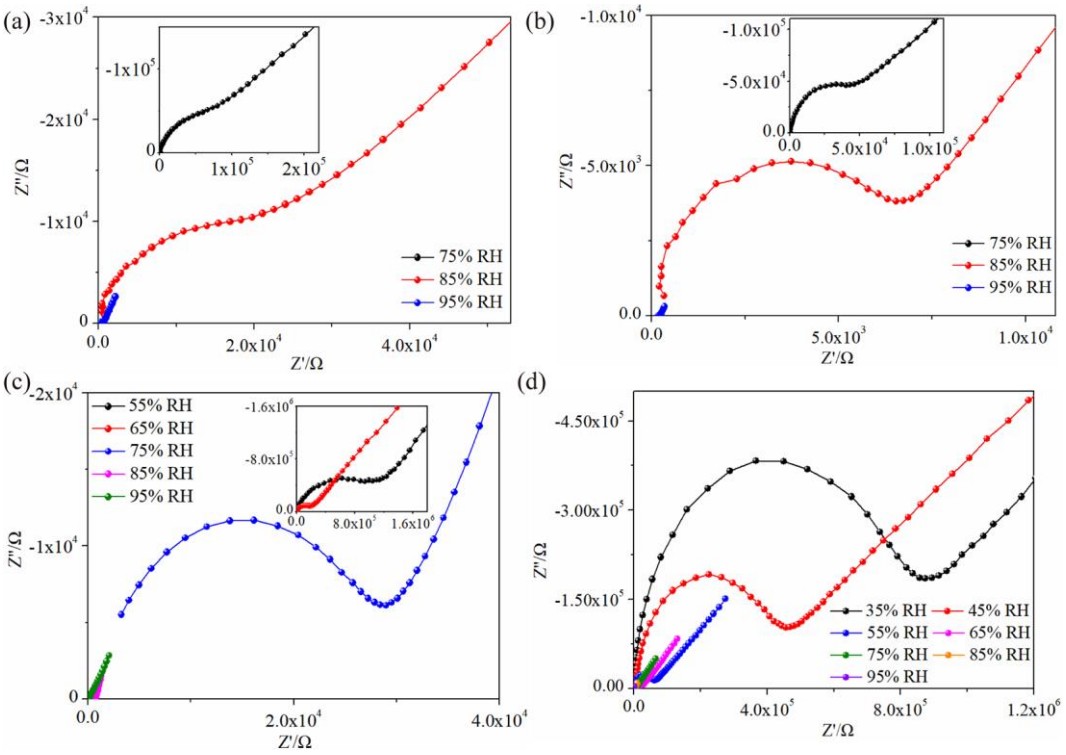

Fig. S11 Nyquist curves of **VB-Gl-x** at 25 ℃ and different relative humidity. (a) **VB-Gl-0.3%**; (b) **VB-Gl-0.5%**; (c) **VB-Gl-1.0%**; (d) **VB-Gl-1.3%**.

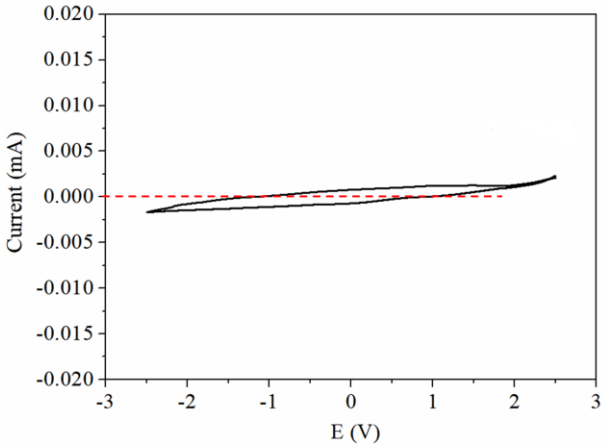

Fig. S12 The CV curve (black) of **VB-Gl-1.3%** under the scan rates of 10 mV/s at room temperature with red level line for comparison.

4. Supplementary Tables

Table S1 Proton conductivities (S cm^{-1}) of reported excellent proton conduction crystalline materials.

Material	Conductivity	Condition	Ref.
1Eu	1.95×10^{-2}	58 °C, 98%RH	*CCS Chem.,* 2022, 4, 2938.
$H_7Na_{19}(H_2O)_{26}\{Ni_{12}(OH)_9(PO_4)_4$(A-α-$SiW_9O_{34})[W_4O_{10}(OH)(PO_2(OH)_2)_2$(A-α-$SiW_9O_{34})_2]\}\cdot4C_2H_8N\cdot27H_2O$	1.89×10^{-2}	50 °C, 98% RH	*Inorg. Chem. Front.,* 2021, 8, 1303.
$[La_{27}Ge_{10}W_{106}O_{406}(OH)_4(H_2O)_{24}]^{59-}$	1.5×10^{-2}	85 °C, 98% RH	*Angew. Chem. Int. Ed.,* 2017, 56, 2664.
VB ([100] direction)	1.25×10^{-2}	55 °C, 95%RH	**This work**
$[(CH_3)_4N]_{1.5}K_{5.5}Na_2[I_3\subset(MoV_2O_2S_2)_{8-}(Se^{IV}O_3)_8(OH)_8]\cdot25H_2O$	1.20×10^{-2}	55 °C, 97%RH	*Adv. Mater.,* 2013, 25, 6245.
KNaLi-1	7.9×10^{-3}	85 °C, 70% RH	*Angew. Chem.,* 2018, 130, 13230.
$H[Ce(H_2O)_4]_2[MnV_{13}O_{38}]\cdot9NMP\cdot17H_2O$	4.68×10^{-3}	61 °C, 97% RH	*Inorg. Chem. Front.,* 2018, 5, 1213.
$ILMo_{132}$	3.28×10^{-3}	60 °C, 98% RH	*ACS Appl. Mater. Interfaces.,* 2019, 11, 7030.
$\{H_9[Cu(en)_2(H_2O)_2][Cu(en)_2]_{12}[In(en)]_5[Nb_{23}O_{65}(OH)_3(H_2O)_2]\{Nb_{24}O_{67}(OH)_2(H_2O)_3]_2\}\cdot68H_2O$	1.78×10^{-3}	85 °C, 98% RH	*Inorg. Chem.,* 2022, 61, 8112.
Mg-NU-225 (perpendicular directions)	1.6×10^{-3}	55 °C, 95% RH	*Inorg. Chem.,* 2021, 60, 1086.
$[Co(bpz)(Hbpz)][Co(SO_4)_{0.5}(H_2O)_2(bpz)]_4[PMo^{VI}_8Mo^{V}_4V^{IV}_4O_{42}]\cdot13H_2O$	1.5×10^{-3}	75 °C, 98% RH	*Chem. Eur. J.,* 2016, 22, 9299–9304.
$[Cu_2(Htzehp)_2$(4,4′-bipy)$]\cdot3H_2O$	1.43×10^{-3}	80 °C, 95% RH	*Chem. Mater.,* 2017, 29, 2321.

([100] direction)			
$[Cu_2(Htzehp)_2(4,4'\text{-bipy})]\cdot 3H_2O$ ([010] direction)	2.5×10^{-5}	80 °C, 95% RH	*Chem. Mater.,* 2017, 29, 2321.
$TBAMo_{132}$	1.8×10^{-5}	60 °C, 98% RH	*ACS Appl. Mater. Interfaces,* 2019, 11, 7, 7030.
Mg-NU-225 (parallel directions)	1.5×10^{-5}	55 °C, 95% RH	*Inorg. Chem.,* 2021, 60, 1086.
$[H_2en]_4[Ni_5(OH)_3(trzS)_3(en)(H_2O)(B\text{-}\alpha\text{-}PW_9O_{34})]\cdot 6H_2O$	1.3×10^{-5}	85 °C, 98% RH	*Chem. Commun.,* 2015, 51, 2048.

Table S2 Proton conductivities (S cm^{-1}) of **VB**, and composite proton conductors with different Gl content under 95% RH.

Sample	25 ℃ (S cm^{-1})	35 ℃ (S cm^{-1})	45 ℃ (S cm^{-1})	55 ℃ (S cm^{-1})	65 ℃ (S cm^{-1})	75 ℃ (S cm^{-1})	85 ℃ (S cm^{-1})
VB	1.40×10^{-5}	2.07×10^{-5}	2.96×10^{-5}	7.99×10^{-5}	5.18×10^{-5}	—	—
VB-Gl-0.3%	3.74×10^{-4}	6.78×10^{-4}	8.01×10^{-4}	1.03×10^{-3}	1.02×10^{-3}	—	—
VB-Gl-0.5%	5.13×10^{-4}	8.09×10^{-4}	1.19×10^{-3}	1.53×10^{-3}	1.44×10^{-3}	—	—
VB-Gl-1.0%	1.37×10^{-3}	2.84×10^{-3}	3.87×10^{-3}	4.62×10^{-3}	4.87×10^{-3}	5.13×10^{-3}	5.11×10^{-3}
VB-Gl-1.3%	2.45×10^{-3}	3.06×10^{-3}	4.31×10^{-3}	5.78×10^{-3}	7.53×10^{-3}	1.16×10^{-2}	1.28×10^{-2}

Table S3 Proton conductivities (S cm^{-1}) of **VB**, and composite proton conductors with different Gl content at 25 ℃ and different relative humidity.

Sample	35% RH	45% RH	55% RH	65% RH	75% RH	85% RH	95% RH
VB	—	—	—	—	1.65×10^{-6}	5.16×10^{-6}	1.40×10^{-5}
VB-Gl-0.3%	—	—	—	—	2.28×10^{-6}	1.08×10^{-5}	3.73×10^{-4}
VB-Gl-0.5%	—	—	—	—	2.56×10^{-6}	1.80×10^{-5}	5.13×10^{-4}
VB-Gl-1.0%	—	—	1.19×10^{-7}	6.45×10^{-7}	4.67×10^{-6}	1.87×10^{-4}	1.38×10^{-3}
VB-Gl-1.3%	1.82×10^{-7}	3.49×10^{-7}	2.53×10^{-6}	6.94×10^{-6}	3.38×10^{-5}	2.19×10^{-4}	2.45×10^{-3}